



Design, synthesis, and in silico-in vitro antimalarial evaluation of 1,2,3-triazole-linked dihydropyrimidinone quinoline hybrids

Rasheed A. Adigun¹ · Frederick P. Malan¹ · Mohammed O. Balogun² · Natasha October¹

Received: 26 December 2022 / Accepted: 7 February 2023
© The Author(s) 2023

Abstract

In response to the malaria parasite's resistance towards quinoline-based antimalarial drugs, we have employed quinoline-containing compounds in combination with dihydropyrimidinone (DHPM) analogues as resistance reversal agents (RAs) and investigated their antimalarial activities based on DHPM's resistance reversal abilities. The present study employed click chemistry to link DHPM and quinoline compounds which offered several synthetic advantages over the previously used amide coupling for the same hybrids. Among the synthesised compounds, 4 hybrids with the 7-chloroquinoline moiety showed antimalarial activity below 1 μM while compounds with the mefloquine moiety showed lower antimalarial activity than chloroquine (CQ) and the 7-chloroquinoline hybrids. Among the tested hybrids for the IC_{50} determination, four compounds displayed good antimalarial activity with increased sensitivity against the CQ-resistant K1 strain between 421 and 567 nM and showed higher activity between 138 and 245 nM against the NF54 CQ-sensitive strain, while three compounds have IC_{50} values greater than 5 μM . Additionally, in silico molecular docking and molecular dynamics studies were conducted to investigate the binding affinities of all the synthesised compounds as glutathione reductase protein competitive inhibitors. Further optimisation of the compound with the highest binding affinity generated 16 compounds with higher binding affinities than the flavine adenine dinucleotide (FAD) cofactor.

Keywords Antimalarial · Click chemistry · Dihydropyrimidinone · Resistance reversal · In silico

Introduction

Recent data indicates that the challenge to overcome malaria still lingers [1], regardless of all the significant efforts and advances in drug developments and medical technologies. The rise of drug or multidrug resistance in *Plasmodia strains* has made malaria the most important tropical parasitic disease [2]. Therefore, developing new antimalarial drugs is necessary to rectify this situation. Despite the development

of many antimalarial leads, quinoline compounds remain important in malarial chemotherapy [3].

For many years, chloroquine (CQ) from the quinoline family was the first-line antimalarial drug. Despite the huge success recorded in using quinoline for malaria therapeutics, these drugs have been challenged by *Plasmodium* parasites due to their rapid development of resistance [4, 5]. Drug resistance in malaria occurs when the parasite strain continues to multiply or survive even though the therapeutic has been given in the recommended tolerable dose. This situation is not malaria-specific but is also observed in cancer and other parasitic diseases like the case with antibiotics. As for the case of chloroquine (CQ) resistance, there is strong evidence through different research that resistant malaria parasites accumulate less CQ in their food vacuole than sensitive parasites [6]. This could result from an efflux pumping system, reduced CQ uptake by the parasite, or a combination of both processes [7]. This implies that CQ concentration does not reach the parasite's lethal dose, thereby resulting in its continuous survival.

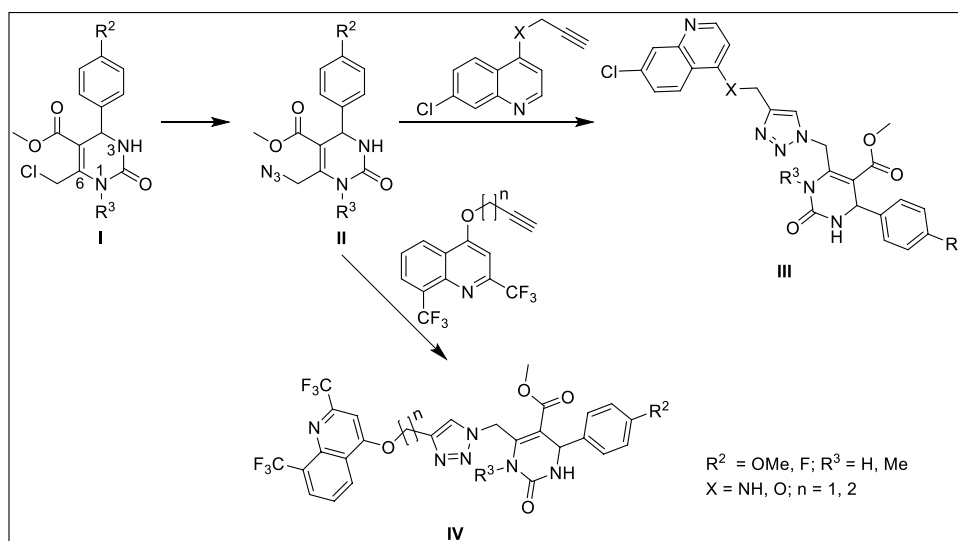
✉ Rasheed A. Adigun
rasheed.adigun@tuks.co.za

✉ Natasha October
natasha.october@up.ac.za

¹ Department of Chemistry, University of Pretoria, Lynnwood Road, 0002 Hatfield, Pretoria, South Africa

² Biopolymer Modification & Therapeutics Lab, Chemicals Cluster, Council for Scientific and Industrial Research, Meiring Naude Road, 0001 Brummeria, Pretoria, South Africa

Scheme 1 General structure of the target DHPM hybrids based on CQ (**III**) and mefloquine (**IV**)



The use of resistance reversal agents (RAs) is among the strategies to reverse this drug resistance in malaria parasites. Resistance reversal refers to the use of a compound that can restore the sensitivity of resistant strains to a drug while it might have little or no therapeutic action against the parasite [8]. In the context of malaria, resistance RAs ensure antimalarial drugs accumulate within the parasite's food vacuole. An interesting feature of this strategy is the ability to combine two biologically active compounds in a hybrid, maintaining the properties of both without the setback of differing elimination half-life ($t_{1/2}$) or pharmacokinetic properties associated with separate drugs that are used in combination therapy. Furthermore, a major advantage of this approach over the rest is the ability of the RA to competitively bind to the *P. falciparum* chloroquine resistance transporter (*Pf*/CRT) protein, thereby inhibiting the efflux of the CQ from the digestive food vacuole of the *Plasmodium* parasite. In contrast, other strategies lack this feature to bind to the mutated CQ-resistant *P. falciparum* [9, 10].

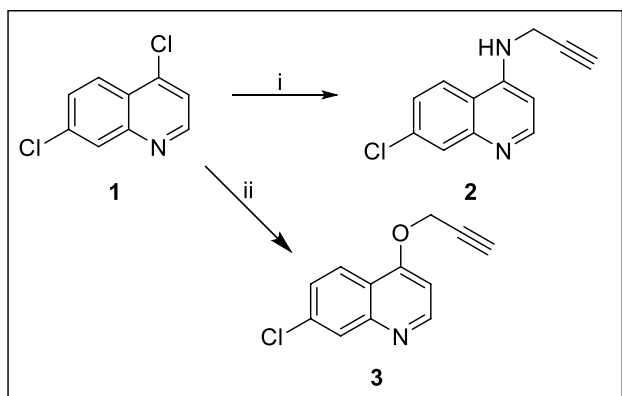
Previously, it was discovered that concurrent exposure of resistant strains of *P. falciparum* to both CQ and verapamil reversed resistance in vitro [4, 11]. Since verapamil is a calcium channel blocker used to treat hypertension and other cardiovascular diseases, researchers have used different calcium channel blockers and other drugs in combination with quinoline-based antimalarial drugs in attempts to reverse antimalarial drug resistance. It was observed that the RA combinations were able to increase the sensitivity of cloned CQ-resistant *P. falciparum* strains in vitro but did not affect the sensitivity of CQ-sensitive strains [6, 11–13].

Before Peyton and co-workers coined the term “Reversed Chloroquine” (RCQ) to describe a hybrid compound containing CQ and an RA, the use of RAs in antimalarial chemotherapy involved the administration of the two agents as separate doses [14]. They discovered

that covalently linking a CQ-like moiety to imipramine was effective against both sensitive and resistant strains of the *Plasmodium* parasite. The hybrid molecule delivered the RA in a 1:1 ratio to the antimalarial quinoline, which would lower the dose required if the two drugs, was to be given in separate forms, with resultant lower cost and toxicity [4]. This arrangement would favour the drug accumulation in the parasite's digestive vacuole and also interfere with the CQ export by the mutated CQ-resistant *P. falciparum* [14].

In our previous work, we covalently linked CQ to dihydropyrimidinone (DHPM) using an amide bond linker at position 3 of the DHPM. The resulting hybrids could reverse resistance in the K1 strain of *P. falciparum* in vitro [15]. Since DHPMs present various sites of functionalisation that could be used for structure–activity relationship (SAR), several synthetic strategies could be employed to link quinoline-based antimalarials to various DHPM scaffolds.

The previous report of the synthesis of DHPM-based hybrids of chloroquine (CQ) moiety used amide coupling to link the CQ to DHPM, specifically at N3 of the reversal agent [15]. The synthetic route to these hybrids involved the protection of N1 nitrogen with a methyl group. Furthermore, the synthesis of the amide carbamate ester intermediate involved overnight reflux with a large excess of phenyl chloroformate and NaH, 10.0, and 11.0 molar equivalents, respectively. This synthetic procedure generated a lot of waste. However, we report on the use of click chemistry as an alternative route to synthesise DHPM-based quinoline hybrids and their antimalarial activities. This project employs a triazole covalent linker between quinoline-based compounds and different DHPMs using the C6 of the DHPM as the point of attachment. Two series of quinoline-based compounds related to chloroquine and mefloquine antimalarial drugs were chosen (Scheme 1)



Scheme 2 Synthesis of quinolines **2** and **3**. Reagent and conditions: (i) propargylamine, 110 °C, N₂, 18 h. (ii) propargyl alcohol, NaH, DMF, 0 °C, 50 °C

It also has been demonstrated that quinoline derivatives block the *P. falciparum* glutathione reductase (*PfGR*) enzyme [16]. The host erythrocytes undergo significant structural and physiological changes when invaded by *P. falciparum* to aid the parasites' survival and growth. The oxidative stress caused by these changes affects the malaria parasites. As a result, an effective antioxidant is necessary to inhibit reactive oxygen species from harming the parasites [17]. It is thought that reduced glutathione (GSH) is a crucial antioxidant during erythrocytic infection. As an oxidoreductase, glutathione reductase in *P. falciparum* converts oxidised glutathione (GS-SG) to reduced GSH using hydrogen from nicotinamide adenine dinucleotide phosphate (NADPH). The transfer of hydrogen from NADPH to GS-SG is the most essential task of the FAD cofactor in *PfGR* because, without it, the parasite would experience oxidative stress [18, 19]. Thus, *P. falciparum*'s glutathione reductase enzyme becomes a crucial target in antimalarial treatment [20]. Therefore, in addition to the *in vitro* antimalarial testing, the binding affinities and the molecular

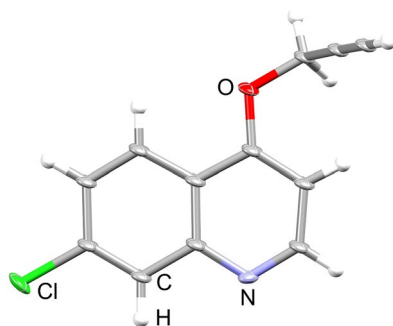
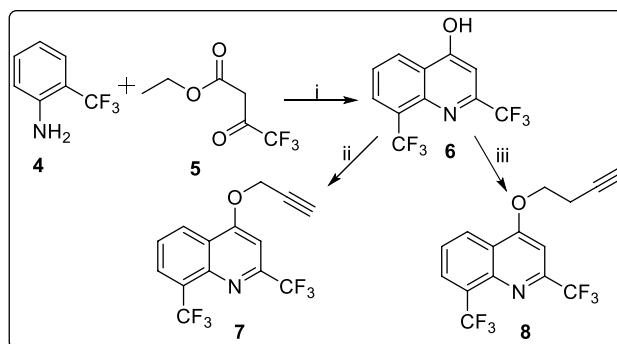


Fig. 1 Molecular structure of compound **3**. Thermal ellipsoids are drawn at a 70% probability level



Scheme 3 Synthesis of 2,8-bis(trifluoromethyl)quinolines. Reagents and conditions: (i) polyphosphoric acid, 150 °C, 3 h; (ii) K₂CO₃, dry DMF, 30 °C, 30 min, propargyl bromide, 6 h; (iii) butyn-1-ol, PPh₃, DEAD, dry THF, 0 °C, 25 °C, 12 h

stabilities of the synthesised compounds within the glutathione reductase enzyme were estimated using molecular docking and molecular dynamics *in silico* methods.

Results and discussion

Chemistry

The synthesis of the chlorinated DHPM and the subsequent azidation to form azides **9a-d** was reported earlier [21]. The terminal alkynes were installed on the quinoline-based compounds using different protocols. Compound **2** was synthesised via a nucleophilic substitution reaction from 4,7-dichloroquinoline **1** according to the reported protocol (Scheme 2) [22]. This involved heating a mixture of **1** and propargylamine in a sealed tube under a nitrogen atmosphere.

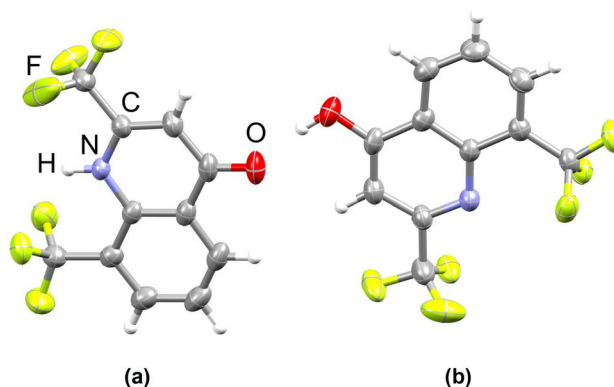


Fig. 2 Molecular structure of compound **6** showing the two tautomers, the keto (**a**) and the enol (**b**) forms. Thermal ellipsoids are drawn at a 50% probability level

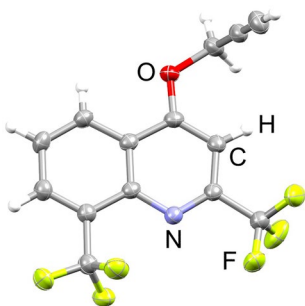
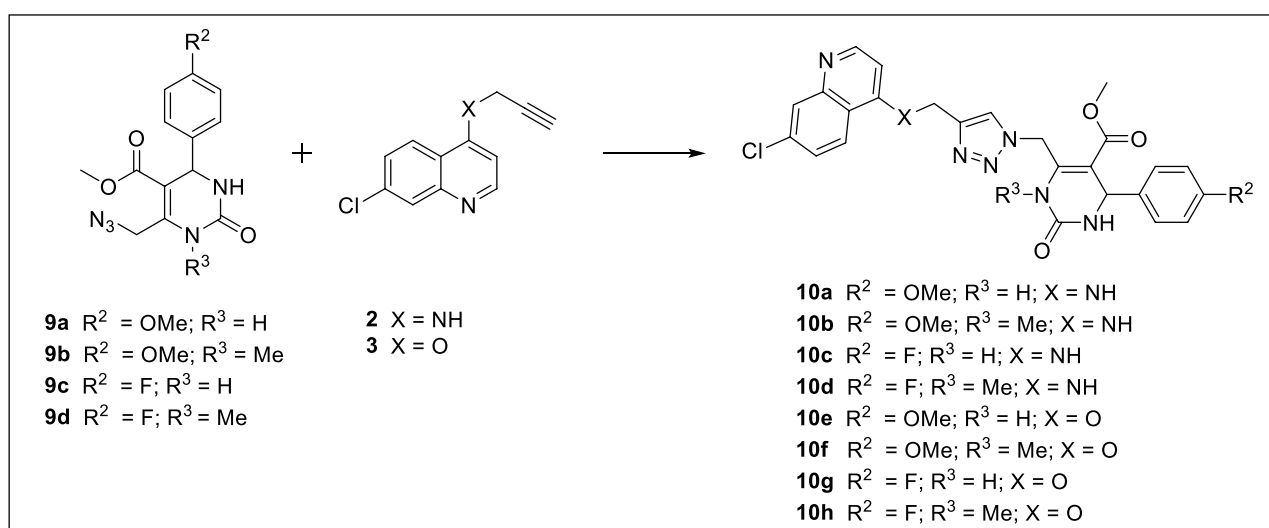


Fig. 3 Molecular structure of compound **7**. Thermal ellipsoids are drawn at a50% probability level

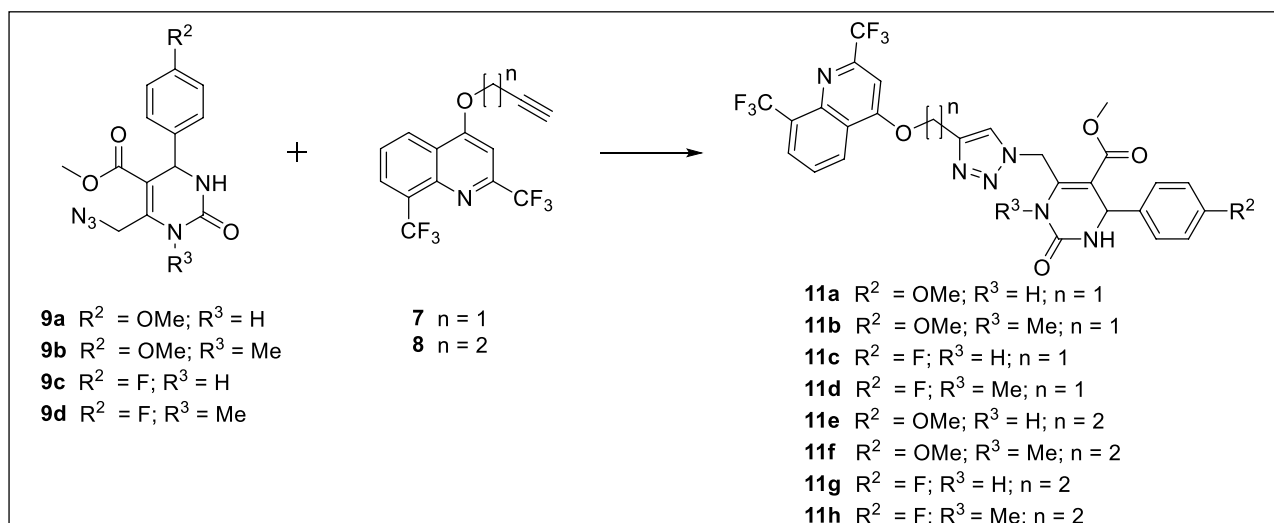
Formation of product **2** was confirmed by ^1H NMR spectroscopy with the observance of the terminal alkyne's proton at δ_{H} 2.66 ppm (t, $^4J_{\text{HH}}=2.5$ Hz). The method reported by Kaval et al. was adapted to synthesise the oxyquinoline **3** (Scheme 2) [23]. The formation of compound **3** was confirmed from the ^1H NMR spectrum with the terminal alkyne's proton appearing at δ_{H} 2.62 ppm (t, $^4J_{\text{HH}}=2.4$ Hz) and the Single crystal X-ray diffraction (SCXRD) technique (Fig. 1). The quinolinol **6** was synthesised via Conrad-Limpach synthesis of quinolines, which was readily converted to the alkynes **7** and **8** (Scheme 3).

Aniline **4** was quantitatively cyclised to the quinolinol **6** by heating it at 150 C with ethyl 4,4,4-trifluoroacetate (**5**) for 3 h in the presence of polyphosphoric acid (PPA) as the catalyst [24]. The nucleophilic alkylation of **6** to **7** was performed using the Williamson ether synthesis [25]. To extend the carbon chain linker, compound **8** was synthesised from the quinolinol **6** via the Mitsunobu reaction [26] as Williamson's nucleophilic alkylation of the quinolinol **6** with excess

4-Bromo-1-butyne failed to give the desired product. From the mechanism of Conrad-Limpach synthesis of the quinolines [27, 28], it is possible to obtain two tautomers for the quinolinol **6**: the enol (a) and the keto (b) (Fig. 2). The simultaneous presence of both tautomers was confirmed from the SCXRD data (Fig. 2). It corroborated the earlier isolation by Sarojini et al. [29], but the subsequent deprotonations only involved the enol (a) as was observed from the SCXRD of compound **7** (Fig. 3). The involvement of the enol form for the subsequent deprotonations points to its preference over the keto form. The more stable enol tautomer is not unexpected for two reasons: enol stability by conjugation with a neighbouring pi system and aromaticity [30]. The two factors are present as the quinoline moiety is highly conjugated in the two rings, and they both contain aromatic systems for additional resonance stability. The structure of compound **8** was confirmed from the ^1H NMR spectrum with the observation of all the diagnostic peaks. The terminal alkyne proton appeared at δ_{H} 2.10 ppm (t, $^4J_{\text{HH}}=2.7$ Hz), while the two methylene protons were assigned to the signals δ_{H} 2.90 ppm (td, $^3J_{\text{HH}}=6.7$ Hz, $^4J_{\text{HH}}=2.7$ Hz) and 4.41 ppm (t, $^3J_{\text{HH}}=6.7$ Hz). All the aromatic protons were also observed at the expected peak positions. The hybrid compounds were synthesised by click chemistry reactions (Schemes 4 and 5) as adapted from Guantai et al. [31]. The reaction was first attempted in a mixture of *tert*-butanol and water using copper(I) iodide (CuI) as the catalyst. This gave three spots on the TLC, and no attempt was made to separate them because of their close R_f values. The catalyst was changed to freshly prepared 1-M solution of copper(II) sulphate pentahydrate ($\text{CuSO}_4 \cdot 5\text{H}_2\text{O}$) and sodium ascorbate which reductively produces the required Cu(I) in situ. Initially, this approach seemed to work for the reaction where only one prominent spot was observed on the TLC. However,



Scheme 4 Synthesis of the triazoles 10a-h. Reagents and conditions: CuSO_4 , sodium ascorbate, DMF, H_2O , 25 °C, 12 h



Scheme 5 Synthesis of the triazoles **11a-h**. Reagents and conditions: CuSO_4 , sodium ascorbate, DMF, H_2O , 25°C , 12 h

a difficult-to-filter precipitate also formed from the solution. Another setback was the persistent appearance of the starting materials even after long hours of stirring at 25°C . The solvent was changed to DMF with the catalyst freshly prepared in distilled water. The reaction mixture was stirred for 12 h, and the TLC analysis showed a single spot for the product with complete consumption of the starting materials.

The ^1H NMR spectra obtained for **11a-h** correlated well with the proposed structures, and all the diagnostic peaks were observed (see the supplementary information

for details). Additionally, the predicted connectivity of the compounds was confirmed from the SCXRD structure elucidations of **11d** and **11g** (Fig. 4).

Antimalarial activity of DHPM-quinoline triazole hybrids

The percent growth inhibitory activities of DHPMs **9a-d** and hybrids **10a-h** and **11a-h** were evaluated at $1\text{-}\mu\text{M}$ and $5\text{-}\mu\text{M}$ concentrations in an in vitro antiplasmodial assay (Fig. 5,

Fig. 4 Molecular structures of compounds **11d** (a) and **11g** (b). Thermal ellipsoids are drawn at a 50% probability level

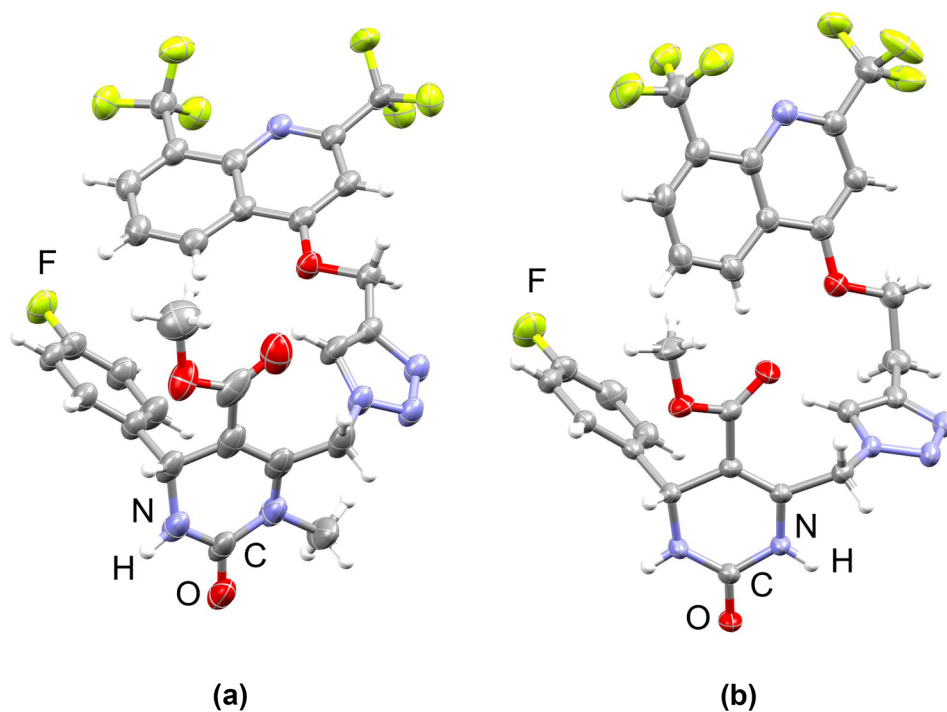


Fig. 5 In vitro activity of DHPM-CQ triazole hybrids at 1 μ M and 5 μ M against asexual *P. falciparum* (NF54 and K1)

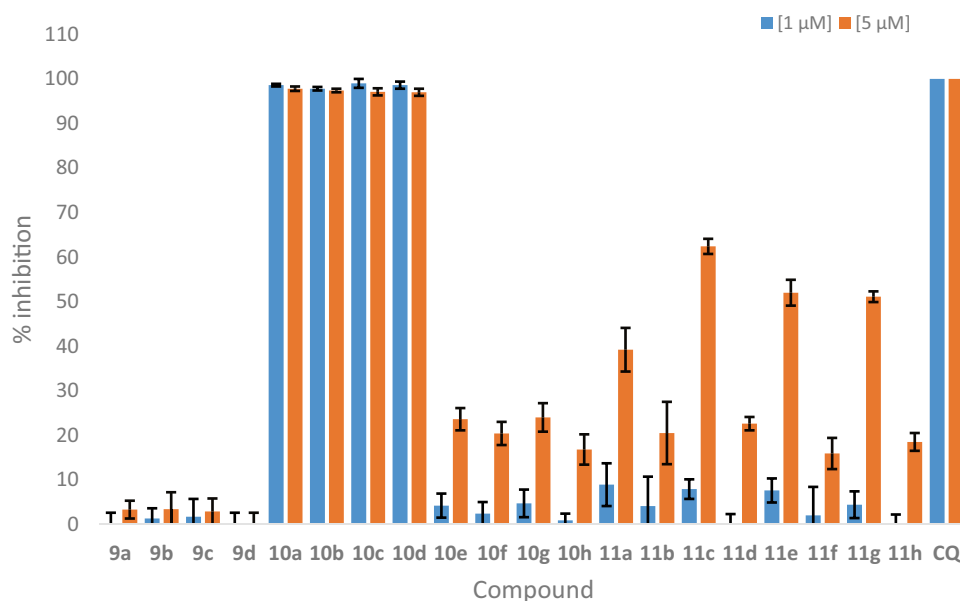


Table 1). An NF54 CQ-sensitive (CQS) *P. falciparum* asexual strain was used. The most potent compounds **10a-d** were further evaluated for the IC_{50} against NF54 CQS, and K1 CQ-resistant (CQR) strains, while the IC_{50} of the moderately potent compounds **11c**, **11e**, and **11g** were determined against the K1 CQR strain only. In all the assays, CQ was used as the reference drug (Table 2).

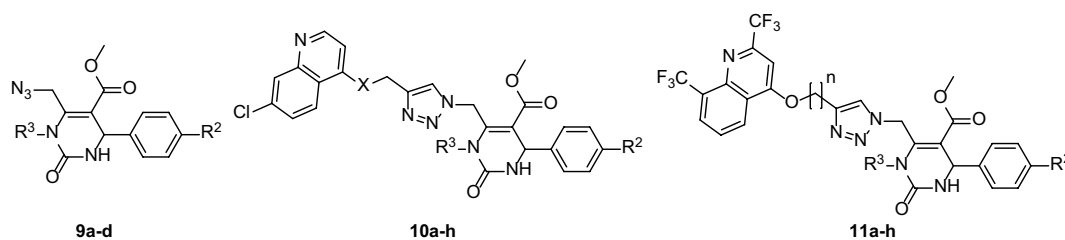
Among the compounds tested against the NF54 strain to determine the percentage inhibition, the reversal agents (RAs) **9a-d** displayed minimal inhibition (Fig. 5, Table 1). This was expected as they lack the antiplasmodial quinoline moiety, and their role in the hybrids is to inhibit the underlying process responsible for drug resistance. Within the same series, compounds **10a-d** with 4-amino functionality displayed the highest inhibitions and were comparable to CQ at the two concentrations tested. Compounds **10e-f** with the 4-oxyquinoline moiety exhibited very low inhibitions, even at 5 μ M. The decrease in the activity of these oxygen-containing hybrids **10e-f** could be attributed to the absence of the 4-amino functionality, which is present in compounds **10a-d**. This agrees with previous reports that quinolines containing an amino group at the 4-position show higher antiplasmodial activities than those containing oxygen or lacking the 4-amino group [32–35]. This stresses the importance of the 4-amino moiety in maintaining the basic property required for the CQ and its analogues to accumulate in the food vacuole of *P. falciparum* [34]. Compounds **11a-h** with the mefloquine moiety showed lower antiplasmodial activity than CQ and the hybrids **10a-h**. Among these hybrids, compounds **11a**, **11c**, **11e**, and **11g**, with unsubstituted acidic protons at N1 and N3, showed better activities than compounds **11b**, **11d**, **11f**, and **11h** which instead have a methyl group at N1. The generally lower activities of

hybrids **11a-h** could also be ascribed to the lack of 4-amino functionality in the quinoline ring [34].

Compounds **10a-d** displayed good antiplasmodial activities against the CQR K1 strain. The IC_{50} s for this strain were between 421 and 567 nM, but much greater potencies of 138–245 nM were observed against the NF54 CQS strain. Compounds **11c**, **11e**, and **11g** were at least three orders of magnitude weaker. Hybrids **10b** and **10d**, containing chloroquine moiety with a methyl group at N1 of the DHPM, showed better antiplasmodial activities than hybrids **10a** and **10c** with unsubstituted acidic protons at N1 and N3 in both NF54 and K1 strains. This higher antiplasmodial activity could result from the decreased acidity associated with the removal of the acidic proton, which increases the basic property of the quinoline hybrid needed for its accumulation in the acidic food vacuole of the *P. falciparum* [36]. In addition, replacing the acidic proton with a methyl group increases the lipophilicity and in turn increases the antimalarial activities [37]. However, other substitutions, particularly the *para*-methoxy and the *para*-fluoro groups on the DHPM aromatic, do not seem to influence the activities of the hybrid compounds. Hybrids **10a-d** also showed reduced Resistance indices (RI) factor ranging from 2.3 to 3.6 as compared to CQ with an RI factor of 8.5. The reduced RI factor suggests that the addition of the DHPM to the quinoline scaffold was able to change the sensitivity of the K1 strain observed.

In silico study

Using the Maestro tool from the Schrödinger software, we performed the in silico study utilising the crystal structure of glutathione reductase (PDB ID: 1ONF). The X-ray

Table 1 In vitro activity of DHPM-CQ triazole hybrids against asexual *P. falciparum* parasites, obtained at concentrations of 1 μM and 5 μM . (CQ was used as a positive control)

Compound	R ²	R ³	X/n	% inhibition [1 μM]		% inhibition [5 μM]	
				Average	$\pm\text{SEM}$	Average	$\pm\text{SEM}$
9a	OMe	H	-	0	2.6	3.3	2
9b	OMe	Me	-	1.3	2.3	3.4	3.8
9c	F	H	-	1.7	4	2.9	2.9
9d	F	Me	-	0	2.6	0	2.6
10a	OMe	H	X = NH	98.6	0.3	97.8	0.5
10b	OMe	Me	X = NH	97.8	0.4	97.4	0.4
10c	F	H	X = NH	99	1	97.1	0.8
10d	F	Me	X = NH	98.6	0.8	97	0.8
10e	OMe	H	X = O	4.2	2.7	23.6	2.5
10f	OMe	Me	X = O	2.4	2.6	20.4	2.6
10g	F	H	X = O	4.7	3.1	24	3.2
10h	F	Me	X = O	0.9	1.5	16.8	3.4
11a	OMe	H	n = 1	8.9	4.8	39.2	4.9
11b	OMe	Me	n = 1	4.1	6.6	20.5	7
11c	F	H	n = 1	7.9	2.2	62.4	1.7
11d	F	Me	n = 1	0	2.3	22.6	1.5
11e	OMe	H	n = 2	7.6	2.7	52	2.9
11f	OMe	Me	n = 2	2	6.4	15.9	3.5
11g	F	H	n = 2	4.4	3	51.1	1.2
11h	F	Me	n = 2	0	2.2	18.5	2
CQ				100		100	

crystallographic structure of *P. falciparum* glutathione reductase was retrieved from the Protein Data Bank (PDB, <https://www.rcsb.org/>). The raw protein structure was

Table 2 In vitro IC₅₀ antiplasmodial activity of compounds 10a-d and compounds 11c, 11e, and 11g

Comp.	NF54		K1		*RI
	IC ₅₀ (nM)	$\pm\text{SEM}$	IC ₅₀ (nM)	$\pm\text{SEM}$	
10a	244.77	29.02	567.23	25	2.3
10b	180.33	18.22	421.67	43.19	2.3
10c	216.63	4.95	551.07	31.29	2.5
10d	138.03	1.82	498.47	13.94	3.6
11c	ND	-	> 10 μM	-	-
11e	ND	-	> 5 μM	-	-
11g	ND	-	> 5 μM	-	-
CQ	4.2	0.5	35.7	1.7	8.5

ND not determined

*Resistance index (RI) = IC₅₀ K1/IC₅₀ NF54

prepared using the protein preparation wizard of the Schrodinger suite. This was used to assign bond orders, remove water molecules beyond 3 Å, and add H atoms. In addition, both missing side chains and missing loops were added using the Prime. While refining, water orientations were sampled using the PROPKA at a pH of 7.0 for the energy optimisation process and the restrained minimisation was done to confine the root-mean-square deviation (RMSD) of heavy atoms to 0.30 Å using an OPLS4 force field [38]. The active site of the protein residues surrounding the FAD cofactor (the bound ligand) was taken as the binding site, and these residues were used for the preparation of the docking grid using the receptor grid generation panel of the Schrodinger suite. No volume was excluded, and likewise, no constraint was defined. The input ligand structures of the synthesised compounds were built using the LigPrep module of the Schrodinger suite. For each 2D structure, the LigPrep process creates 3D structures with minimised energy, proper bond lengths, and angles. At a physiological pH of 7.0 \pm 0.2, the possible ionisation states for each ligand structure were

generated using the EPIK tool. Lastly, the Glide ligand docking module and the related default force field OPLS4 were used to execute the molecular docking in an extra precision (XP) mode.

The docking simulations of the synthesised compounds were run in the binding site of *P. falciparum* glutathione reductase crystal structure (PDB ID: 1ONF) co-crystallised with FAD cofactor, and the outcomes are shown in Table 3. The binding energy of the ligand–protein complex corresponds to the intensity and affinity of the ligand–protein interaction. The docked complexes were rated according to their lowest energy value (kcal/mol). The negative value of the binding energy increases with the increasing strength of the interaction and vice versa. As expected, the FAD cofactor showed the highest binding affinity at -9.644 kcal/mol, followed by compound **10a** at -8.1 kcal/mol. Accidentally, no correlation was observed between the docking scores

and the antiplasmodial IC_{50} values of the synthesised compounds. As it is well known with competitive inhibitors, it is always a challenge to design compounds that could competitively bind at the active site with higher binding affinity than the cofactor [39]; however, rational optimisations could be a saving grace. Though all the synthesised compounds showed insignificantly lower binding affinity than the FAD cofactor, all of them displayed considerable binding energy, and five of the synthesised compounds showed higher binding affinity than the chloroquine standard.

Analysis of the binding pose of compound **10a** showed different electronic interactions as shown in Fig. 6. The compound was able to make different interactions within the active site of glutathione reductase. The $^+NH_3$ of the Lys151 side chain was able to simultaneously make two π -cation interactions with the phenyl group on the DHPM ring (at 4.69 Å) and the DHPM ring itself (at 4.94 Å), while

Table 3 Docking score in kcal/mol of the synthesised compounds and FAD cofactor.

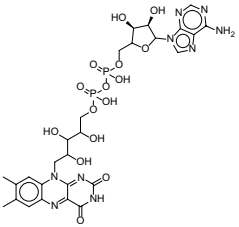
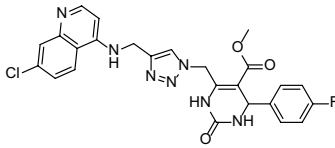
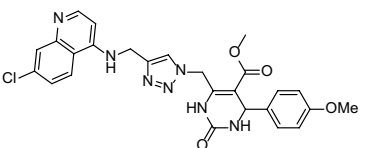
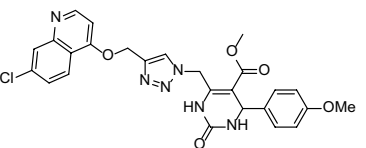
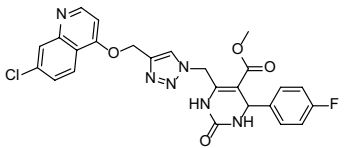
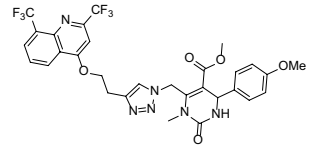
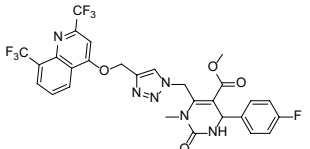
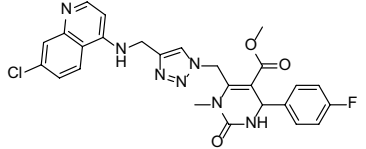
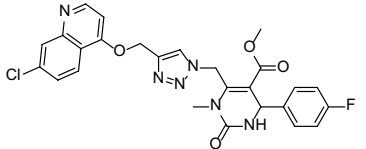
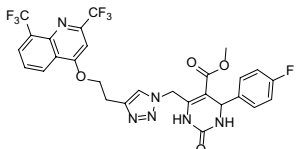
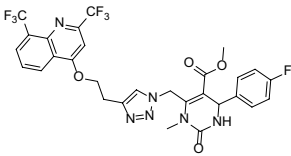
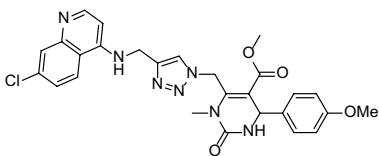
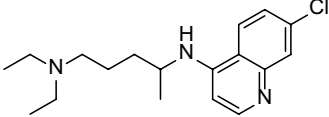
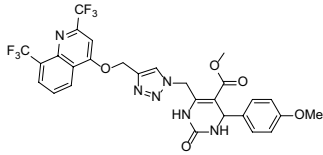
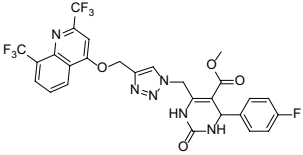
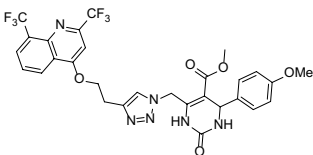
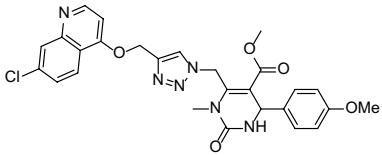
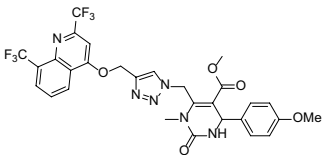
S/N	Ligand	Structure	Docking Score (kcal/mol)	S/N	Ligand	Structure	Docking Score (kcal/mol)
1	FAD		-9.6	10	10c		-6.3
2	10a		-8.1	11	10e		-5.5
3	10g		-7.5	12	11f		-5.0
4	11d		-6.9	13	10d		-4.9
5	10h		-6.8	14	11g		-4.9

Table 3 (continued)

6	11h		-6.7	15	10b		-4.7
7	CQ		-6.5	16	11a		-4.4
8	11c		-6.4	17	11e		-4.0
9	10f		-6.3	18	11b		-2.1

the benzene ring of the quinoline moiety was able to form another π -cation interaction with $^+\text{NH}_3$ side chain of Lys32 (at 3.67 Å). In addition, several H-bond interactions were noted. These include H-bond interactions between N3H of the DHPM and the carboxylic OH of the Asp167 side chain at 1.90 Å, C=O of DHPM, and one NH of the guanidino group of Arg272 side chain at 1.89 Å. Most importantly, the nitrogen of the pyridine ring of the quinoline moiety

was able to form hydrophobically packed H-bond interaction with NH of Ala110 backbone at 1.92 Å (Fig. 7). This type of H-bond is very crucial in maintaining the ligand stability within a protein because of the difficulty involved in breaking the H-bond formed in a hydrophobic space [38]. Another notable feature is the halogen interaction between the chlorine atom on the quinoline and the C=O backbone of Asn278 at 3.36 Å.

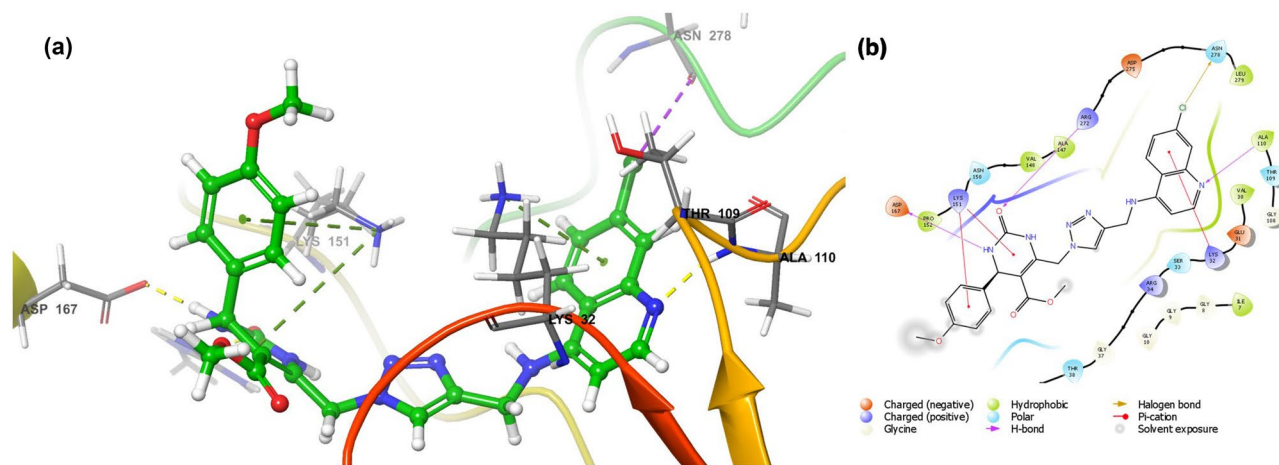
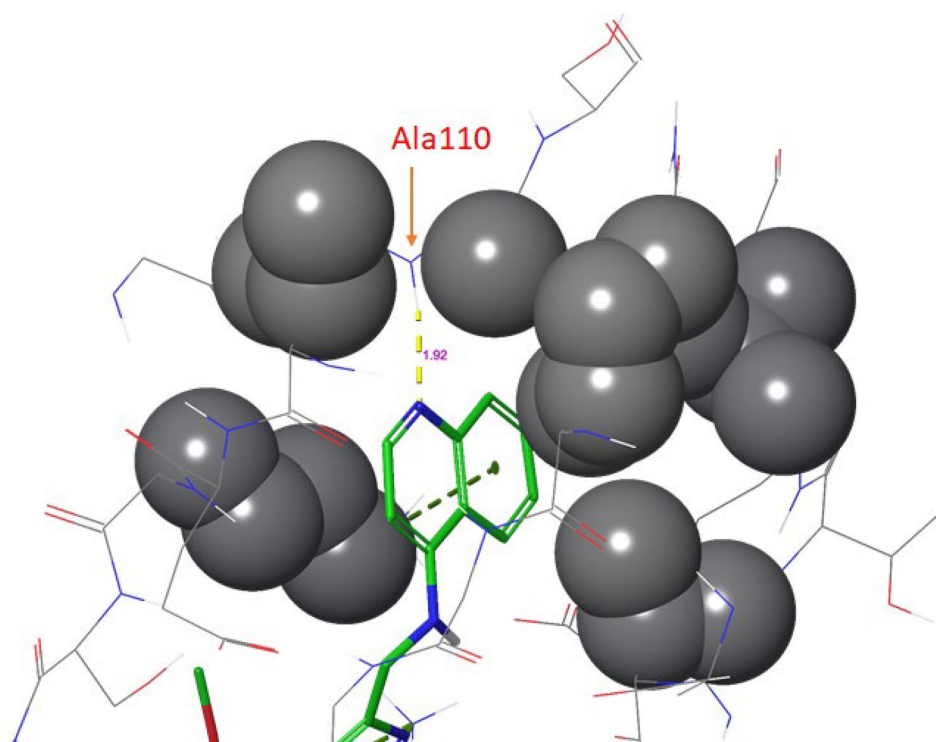


Fig. 6 Binding pose and electronic interactions of compound **10a** within the active site of glutathione reductase. 3D and 2D structures are shown in **a** and **b**, respectively

Fig. 7 Hydrophobically packed H-bond (labelled yellow dotted lines) between Nof the pyridine ring of compound **10a** and Ala110 within the hydrophobic region of glutathione reductase (interacting residues in CPK representation)



Optimisation of compound **10a**

The synthesised compounds must exhibit stronger interactions than the FAD cofactor in order to function as competitive inhibitors at the active site of glutathione reductase. To achieve this, the protein–ligand complex of compound **10a** with the highest binding affinity was loaded onto the workspace and rationally optimised using the Ligand Designer tool in the Maestro platform. Analysis of the workspace showed the 4-methoxy substituent on the phenyl ring of DHPM in a solvent-exposed region. The 4-methoxy group was therefore truncated, leading to an increase in the binding affinity from -8.1 to -8.2 kcal/mol. The growth space of compound **10a**, the ligand–protein interaction, and the truncated **10a** are shown in Fig. 8a, b, and c, respectively.

The light blue regions show the cavity space within the binding pocket, while the deep blue regions show the solvent-exposed areas.

The truncated **10a** was then loaded into the workspace with the protein crystal structure. The pathfinder bonds were activated to identify possible points of R group attachments. With this, the acetate group at position 5 of the DHPM was selected and enumerated to be replaced with the default R groups in Maestro Ligand Designer. The methyl group of the acetate moiety was subsequently replaced and this generated 916 optimised derivatives of compound **10a**. The top 20 ligands are shown in Table 4.

From the generated 916 new ligands, the highest scoring ligand was **LD_350** with a docking score of -11.0 kcal/mol, while ligand **LD_753** had the lowest docking score

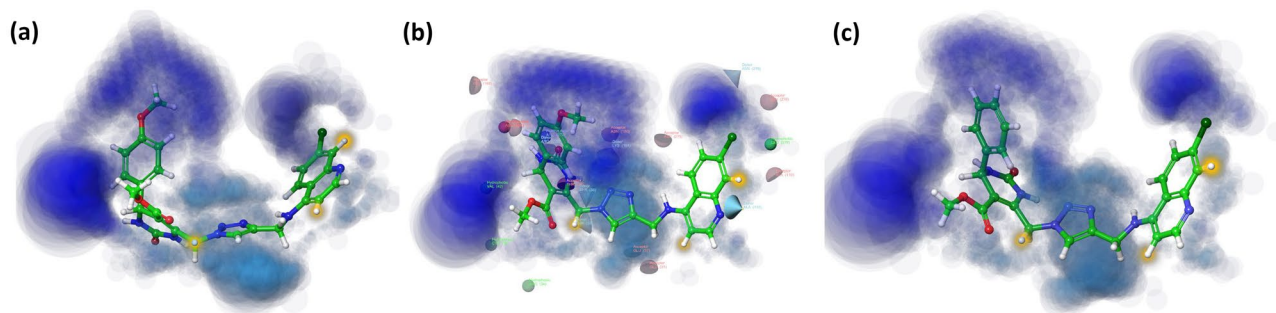


Fig. 8 The growth space of compound **10a** within the glutathione reductase active site (a), the ligand–protein interaction (b), and the truncated **10a** (c)

Table 4 The docking scores of the top 20 optimised ligands in kcal/mol

S/N	Ligand	Structure	docking score kcal/mol
1	LD_350		-11.0
2	LD_762		-10.3
3	LD_865		-10.2
4	LD_344		-10.1
5	LD_228		-10.1
6	LD_922		-10.0
7	LD_771		-10.0
8	LD_129		-9.9
9	LD_482		-9.8
10	LD_459		-9.8

Table 4 (continued)

11	LD_681		-9.8
12	LD_744		-9.8
13	LD_557		-9.8
14	LD_354		-9.7
15	LD_183		-9.7
16	LD_673		-9.6
17	LD_304		-9.6
18	LD_378		-9.6
19	LD_709		-9.6
20	LD_890		-9.6

of -0.3 kcal/mol. The mean was found to be -8.2 kcal/mol, while the median was -8.4 kcal/mol. This indicates that more than 50% of the optimised ligands had higher binding affinity than the original compound **10a** at -8.1 kcal/mol. Interestingly, the optimisation process generated 16 ligands with higher binding affinities than the FAD cofactor, as seen in Table 4. In comparison, 664 ligands had higher binding affinities than the original compound **10a**.

The interaction diagrams of the top two ligands (LD 350 and LD 762) are shown in Fig. 9, showing the changes, especially in the electronic interactions from the added R groups. In LD 350, for example, all the original electronic interactions in compound **10a** were preserved, while the added R group could generate additional H-bond interactions. These are the H-bond between 2-OH of the phenyl ring and C=O backbone of Asp167 at 2.05 Å, the H-bond between 4-OH of the phenyl ring and C=O side chain of Glu168 at 1.55 Å and H-bond between the C=O at the benzyl position and NH side chain of Asn171 at 2.01 Å. These interactions alone with the truncated 4-methoxy group on the DHPM contributed -2.9 kcal/mol of binding energy, which is a 35% increase in binding affinity compared to the original compound **10a**.

Molecular dynamics (MD) simulation

Because molecular docking lacks precise information on the explicit biological water system and the inherent flexibility of the receptor, studies of molecular dynamics that imitate similar biological settings can help to understand the stability of the ligand–protein complex. Based on the docking findings, we ran molecular dynamics simulations for compounds **10a**, LD_350, and LD_762 in this work. The MD simulation was carried out using the Schrödinger Desmond MD simulation software (version 2021–1). To achieve the biological solvation system, the ligand–protein complex was placed in a TIP3P solvation model and then subsequently neutralised by adding 6Cl^- counter ions. The energy minimisation step was also completed to confirm that the system has no steric conflict. The simulation was run for 50 ns at 300 K and 1 bar under an “isothermal-isobaric ensemble” (NPT) condition. The “Nose–Hoover chain thermostat” and “Martyna–Tobias–Klein barostat” approaches were ensemble, respectively, for isothermal-isobaric conditions [40, 41]. At 50-ps intervals, simulation trajectories were obtained, and the resulting trajectories were evaluated.

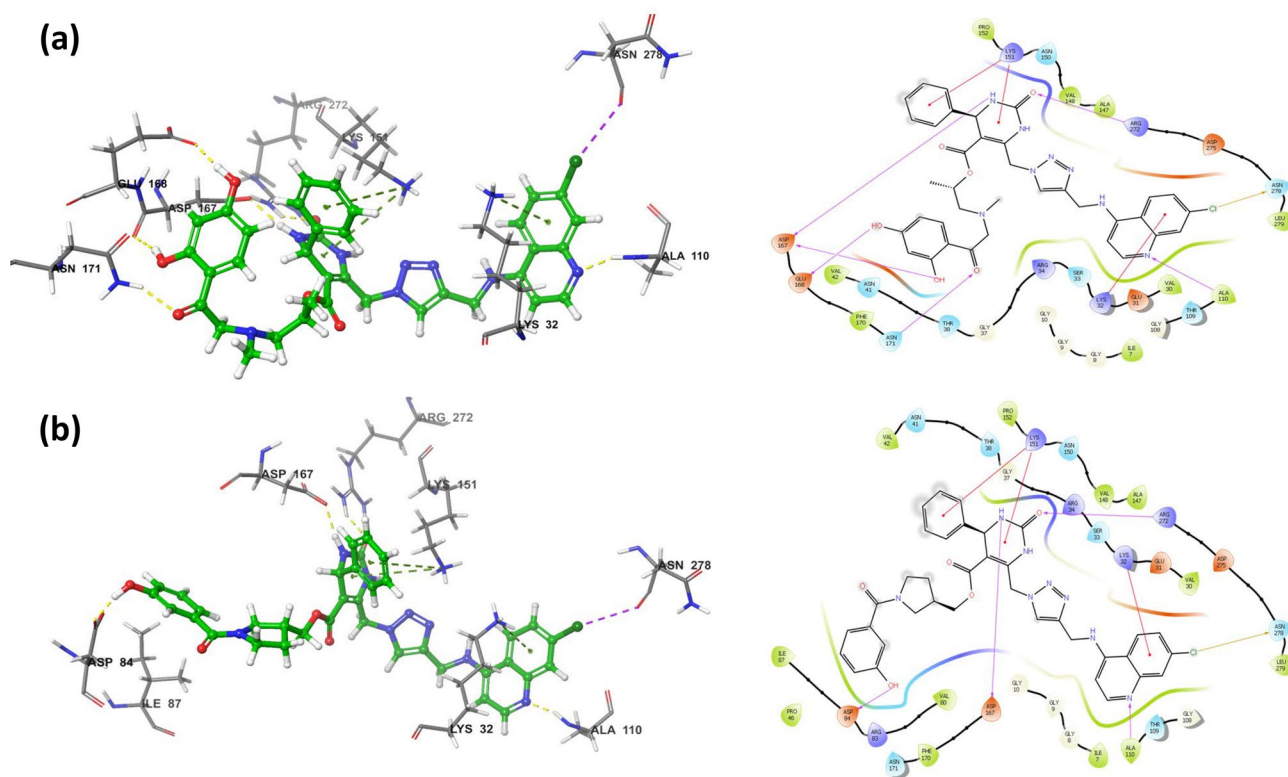


Fig. 9 The interaction diagrams of the top two ligands LD 350 (a) and LD 762 (b)

The MD simulation utilises protein equilibration, flexibility, and the average distance between backbone atoms to calculate the RMSD to estimate the fluctuation of the total protein–ligand complex. A protein–ligand complex with a lower RMSD value indicates a more stable interaction. In the case of compound **10a**, both the protein and the ligand RMSD values lie at approximately 3.0 Å, though the RMSD of the protein averagely lies above 3.0. In contrast, the ligand averagely lies below 3.0 Å except at approximately 35 and 43 ns, where it went slightly above 3.0 Å (See SI Fig. S1a). In addition, the protein and the ligand attained equilibration at less than 5 ns, and no apparent separation between them could be seen throughout the 50-ns MD simulation. Indicating the stability of the original docked structures, the approximately constant RMSD of C α atoms and minor fluctuations of the ligand atoms during the MD simulation show that the conformation of the ligand did not change or varied very little. Comparing this with the RMSD of the optimised ligands, the LD_350 complex (See SI Fig. S1b), for example, showed lower RMSD values at the beginning of the simulation for the ligand but was only able to achieve equilibration at around 37 ns. Though the RMSD of the ligand increased from ~1.8 Å to ~4.2 Å during the equilibration, no separation was observed after the equilibration till the end of the simulation period. The RMSD diagram of LD_762 revealed that the protein–ligand complex achieved equilibration at ~18 ns, and no separation was observed till the end of the simulation period (See SI Fig. S1c). In this case, the protein showed the slightest deviation and had a maximum RMSD value of 2.4 Å till the end of the simulation, while the RMSD value of the ligand was higher at ~5.6 Å at the end of the simulation.

The molecular dynamics simulation identified the major binding interactions between the simulated ligands and glutathione reductase protein. One of the most significant advantages of MD simulation is its ability to precisely identify stable binding interactions from those revealed by molecular docking studies. In most cases, the flexibility of the protein and the ligand in MD, as obtained in a physiological condition, gives rise to the observed differences. In addition, the contact time of each interaction of the ligand with different protein residues as a function of the total simulation period is shown in percentage (See SI Fig. S2). In the case of compound **10a**, for example, the two π -cation interactions between $^+\text{NH}_3$ of Lys151 and the DHPM rings, as shown in molecular docking, were not preserved. The π -cation interaction of the amino side of Lys32 was preserved at 45% of the simulation time but with the triazole ring rather than the benzene ring of the quinoline moiety. Likewise, the halogen bond interaction between Cl of the quinoline moiety and Asn278 was not preserved.

Interestingly, most of the H-bond interactions involving compound **10a** were preserved, and MD was able to identify new H-bond interactions. H-bond interactions involving N3H of DHPM and Asp167 and that of the N of the pyridine ring in quinoline with Ala110 were preserved at 96 and 92%, respectively. In comparison, that of the C=O of the DHPM with Arg272 was lost, but the same C=O was able to form two new H-bond interactions with Thr38 and Asn150 simultaneously at 72 and 94%, respectively. As for the newly identified H-bond interactions, these involved N1H of the DHPM with Gly37 and N3 of the triazole ring with Gly149 at 62 and 32%, respectively. The same trend was observed with the optimised ligands. Analysing LD_350, for instance, the MD did not preserve any of the identified H-bond interactions from the added R-group except for the newly formed intramolecular H-bond interaction between the 2-OH on the benzene ring and its C=O (See SI Fig. S2b). The π -cation interactions between the quinoline rings and Lys32, as well as the DHPM ring and Lys151, are also noteworthy. These were preserved from the molecular docking interactions except for the newly identified π -cation interaction between the pyridine ring of the quinoline moiety and Lys32. Interestingly, the changes in either atomic distances or bond angles beyond the allowed limits resulted in the observed lost interactions in all the cases.

Using the root mean square fluctuation (RMSF) approach, we identified the protein regions exhibiting residue fluctuations across the simulation time. This clarifies how the flexibility of the protein is impacted by ligand binding. As expected, the graphs show the high flexibility of the protein's N and C termini [39]. Although there were non-terminal residues with greater RMSF values, they were either extremely close to the terminal or very far from the protein's binding pocket, as demonstrated by Gly67 in the **10a**-protein complex, which had an RMSF value of 3.29 Å. All the protein residues interacting with the ligands generally displayed variations at a mean value of 1.0 Å (See SI Fig. S3a, b, and c).

Conclusion

Click chemistry has been successfully used to link DHPM to quinoline-based compounds. The use of click chemistry offers several advantages over the previous amide coupling method. These include a better functional group tolerance, ease of synthesis, lesser waste generation, and better atom economy. From the antimalarial results obtained, we have been able to show that the hybrids containing DHPM and 4-aminoquinoline moieties with triazole linker at position 6 of the DHPM showed good antimalarial activity with IC₅₀ values below 1 μM and decreased resistance indices than CQ. In general, hybrids with 4-amino functionality displayed better antimalarial activities than those containing oxygen

at position 4 of the quinoline ring. The hybrids with mefloquine moiety could be modified in the future to include a 4-amino group on the quinoline ring for comparative anti-malarial activities. Apart from position 6 of the DHPM, other positions on the DHPM ring could also be explored to link the quinolines using triazole linkers. Using molecular docking and dynamics approaches, we further explored the synthesised compounds as glutathione reductase inhibitors. Five of the synthesised compounds showed higher binding affinity than the CQ standard, though none showed a higher binding affinity than the FAD cofactor. Rational optimisation of the compound with the highest binding affinity generated 916 ligands, with 664 having higher binding affinities than the original compound and 16 ligands higher than the FAD cofactor. The rational optimisation approach was necessary to produce ligands that could serve as competitive inhibitors of glutathione reductase.

Experimental

General

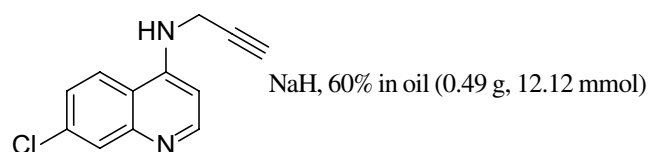
A Gallenkamp melting-point apparatus was used for the melting point determination in open capillary tubes and is uncorrected. ^1H and ^{13}C NMR spectra were recorded on either a Bruker Avance 400 (at 400.21 MHz for ^1H and 100.64 MHz for ^{13}C) or 300 (at 300.13 MHz for ^1H and 75.48 MHz for ^{13}C) spectrometers using CDCl_3 or $\text{DMSO}-d_6$ as solvents at room temperature. Chemical shifts were recorded as part per million (ppm) using tetramethylsilane as an internal standard. 2D NMR experiments were recorded on Bruker Avance 400. Mass analysis was performed on Waters® Synapt G2 High Definition Mass Spectrometry (HDMS) system with flow injection analysis (FIA) using electrospray ionisation (ESI) probe. The MS data were acquired and processed on MassLynx™ software (version 4.1). FT-IR measurements were made on a Bruker Alpha Platinum-ATR spectrometer as neat. All reagents and solvents were purchased from Sigma-Aldrich and used without further purification.

X-ray crystallography

Single-crystal diffraction experiments of compounds **3** and **6** were performed using Quazar multi-layer optics monochromated Cu K α radiation ($k=1.54178 \text{ \AA}$) on a Bruker D8 Venture kappa geometry diffractometer with duo I μ s sources, a Photon 100 CMOS detector and APEX III control software [42]. Data reduction was performed using the SAINT+ [42], and the intensities were corrected for absorption using the SADABS [42]. Single crystals of **7**, **11d**, and **11g** were analysed on a Rigaku XtaLAB Synergy R diffractometer with

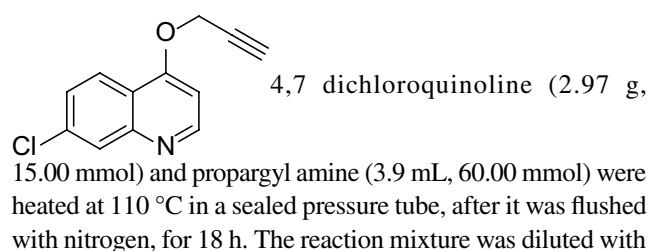
a rotating-anode X-ray source and a HyPix CCD detector. Data reduction and absorption were carried out using the CrysAlis Pro (version 1.171.40.23a) software package [43]. All X-ray diffraction measurements were performed at 150(1) K, using an Oxford Cryogenics Cryostat. All structures were solved by direct methods with SHELXT-2016 [44] using the SHELXL-2016 algorithm [45]. All H atoms were placed in geometrically idealised positions and constrained to ride on their parent atoms. For data collection and refinement parameters, see the SI (Tables S1, S2). The X-ray crystallographic coordinates for all structures have been deposited at the Cambridge Crystallographic Data Centre (CCDC), with deposition numbers CCDC 2076919–2076923. The data can be obtained free of charge from The Cambridge Crystallographic Data Centre via www.ccdc.cam.ac.uk/data_request/cif.

Synthesis of 7-chloro-N-(prop-2-yn-1-yl)quinolin-4-amine (2)



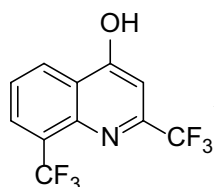
was added to a solution of propargyl alcohol (0.7 mL, 12.12 mmol) in 10.0 mL dry DMF at 0 °C and stirred for 10 min under nitrogen before adding 4, 7-dichloroquinoline (2.06 g, 10.10 mmol) in dry DMF (5.0 mL). The reaction mixture was brought to room temperature and then heated at 50 °C for 3 h at which point the TLC indicated the disappearance of the starting material. The reaction mixture was poured into distilled water (200.0 mL) and extracted with EtOAc (3×50.0 mL). The combined organic layers was washed with brine (50.0 mL) and distilled water (5×50.0 mL), dried with MgSO_4 , and filtered and concentrated in vacuo. The crude residue was purified on column chromatography using SiO_2 gel with 30% acetone in hexane as eluent. White powder: yield 1.04 g, 32%; ^1H NMR (400 MHz, methanol- d_4): δ_{H} 8.42 (d, $^3J_{\text{HH}}=5.6$ Hz, 1H, pyH), 8.03 (d, $^3J_{\text{HH}}=9.0$ Hz, 1H, ArH), 7.80 (d, $^4J_{\text{HH}}=2.1$ Hz, 1H, ArH), 7.41 (dd, $^3J_{\text{HH}}=9.0$, $^4J_{\text{HH}}=2.2$ Hz, 1H, ArH), 6.66 (d, $^3J_{\text{HH}}=5.6$ Hz, 1H, NH), 4.17 (d, $^4J_{\text{HH}}=2.5$ Hz, 2H, CH_2), and 2.66 (t, $^3J_{\text{HH}}=2.5$ Hz, 1H, CH).

Synthesis of 7-chloro-4-(prop-2-yn-1-yloxy)quinoline (3)



methanol and then concentrated in vacuo. The concentrated mixture was diluted with 200.0 mL 1 M NaOH and extracted with EtOAc (3 × 100.0 mL). The combined organic layers were washed with brine (100.0 mL) and distilled water (3 × 50.0 mL), followed by drying with MgSO₄ and filtration. The organic solvent was removed in vacuo to give the crude product which was purified on column chromatography using silica gel with 6% MeOH in DCM as the eluent. White crystals (needles): yield 1.38 g, 63%; m.p. 126–129 °C; FT-IR: ν (cm⁻¹) = 2106 (C≡C); and ¹H NMR (400 MHz, CDCl₃): δ_{H} 8.76 (d, ³J_{HH} = 5.2 Hz, 1H, pyH), 8.13 (d, ³J_{HH} = 8.9 Hz, 1H, ArH), 8.02 (d, ⁴J_{HH} = 2.1 Hz, 1H, ArH), 7.45 (dd, ³J_{HH} = 8.9, ⁴J_{HH} = 2.1 Hz, 1H, ArH), 6.85 (d, ³J_{HH} = 5.3 Hz, 1H, pyH), 4.93 (d, ⁴J_{HH} = 2.4 Hz, 2H, CH₂), and 2.62 (t, ⁴J_{HH} = 2.4 Hz, 1H, CH). ¹³C NMR (101 MHz, CDCl₃): δ_{C} 160.2, 152.3, 149.8, 135.9, 127.9, 126.8, 123.4, 119.7, 101.5, 77.0, 76.9, and 56.2. ESI-HRMS (*m/z*) was calculated for C₁₂H₉ClNO: 218.0373 and found 218.0403 [M + H]⁺.

Synthesis of 2,8-bis(trifluoromethyl)quinolin-4-ol (6)

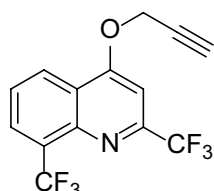


A mixture of 2-trifluoromethyl aniline

(15.08 g, 120.00 mmol), ethyl 4,4,4-trifluoroacetate (17.6 mL, 120.00 mmol), and polyphosphoric acid 115% (75.40 g, 5% w/w) was heated with stirring at 150 °C for 3 h, after which the hot reaction mixture was poured into ice water (600.0 mL) which precipitated the crude product. The precipitate was suction filtered and air dried. The crude product obtained was purified on column chromatography with SiO₂ gel using 2% methanol in DCM as eluent.

Colourless crystals: yield 26.64 g, 79%; ¹H NMR (400 MHz, CDCl₃): δ_{H} 8.62 (d, ³J_{HH} = 8.3 Hz, 1H, ArH), 8.10 (d, ³J_{HH} = 7.4 Hz, 1H, ArH), 7.61 (t, ³J_{HH} = 7.8 Hz, 1H, ArH), 7.45 (s, 1H, pyH), and 6.95 (bs, 1H, OH).

Synthesis of 4-(prop-2-yn-1-yloxy)-2,8-bis(trifluoromethyl)quinoline (7)

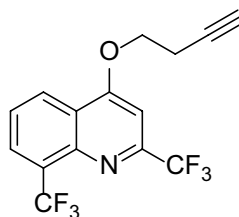


6 (1.50 g, 5.33 mmol) was dissolved in

dry DMF (10.0 mL) and followed by the addition of K₂CO₃ (1.10 g, 8.00 mmol). The reaction mixture was stirred at 30 °C for 30 min. Propargyl bromide (0.9 mL, 10.00 mmol)

was then slowly added and stirring was continued at 30 °C for 6 h under nitrogen. TLC analysis showed the complete conversion of the starting material. The reaction mixture was diluted with distilled water (50.0 mL) and extracted with EtOAc (3 × 30.0 mL). The organic layers were combined and washed with brine (30.0 mL), distilled water (5 × 30.0 mL), dried with MgSO₄, and filtered. The filtrate was evaporated under vacuum and the crude product was purified on column chromatography with SiO₂ using 20% EtOAc in hexane to give the pure product as colourless crystals. Colourless crystals: yield 1.46 g, 86%; ¹H NMR (300 MHz, CDCl₃): δ_{H} 8.49 (d, ³J_{HH} = 7.7 Hz, 1H, ArH), 8.17 (d, ³J_{HH} = 7.3 Hz, 1H, ArH), 7.70 (t, ³J_{HH} = 7.9 Hz, 1H, ArH), 7.30 (s, 1H, pyH), 5.06 (d, ⁴J_{HH} = 2.4 Hz, 2H, CH₂), and 2.70 (t, ⁴J_{HH} = 2.4 Hz, 1H, CH). ¹³C NMR (101 MHz, CDCl₃): δ_{C} 161.6, 149.5 (q, ²J_{CF} = 35.3 Hz), 144.7, 129.4 (q, ³J_{CF} = 5.5 Hz), 128.4 (q, ²J_{CF} = 30.3 Hz), 126.3, 124.9, 122.5, 122.2, 119.7, 98.4 (q, ³J_{CF} = 2.4 Hz), 77.9, 76.0, and 56.9.

Synthesis of 4-(but-3-yn-1-yloxy)-2,8-bis(trifluoromethyl)quinoline (8)



6 (1.50 g, 5.34 mmol), butyn-1-ol

(1.6 mL, 21.36 mmol), and triphenylphosphine (2.80 g, 10.68 mmol) in dry THF (22.0 mL) were cooled to 0 °C. Diethyl azodicarboxylate (DEAD) (3.4 mL, 21.36 mmol) was added dropwise, and the mixture was stirred at room temperature overnight, after which TLC analysis showed complete consumption of the starting material. The reaction mixture was poured into distilled water (100.0 mL) and extracted with EtOAc (3 × 30.0 mL). The combined organic layers were washed with brine (30.0 mL) and distilled water (5 × 30.0 mL), dried with MgSO₄, and filtered and concentrated in vacuo. The crude residue was purified on column chromatography using SiO₂ gel with 15% EtOAc in n-hexane as the eluent. Yellow crystals: yield 1.76 g, 99%; ¹H NMR (300 MHz, CDCl₃): δ_{H} 8.49 (dd, ³J_{HH} = 8.5, ⁴J_{HH} = 1.5 Hz, 1H, ArH), 8.14 (d, ³J_{HH} = 7.3 Hz, 1H, ArH), 7.66 (t, ³J_{HH} = 7.9 Hz, 1H, ArH), 7.13 (s, 1H, pyH), 4.41 (t, ³J_{HH} = 6.7 Hz, 2H, CH₂), 2.90 (td, ³J_{HH} = 6.7, ⁴J_{HH} = 2.7 Hz, 2H, CH₂), and 2.10 (t, ⁴J_{HH} = 2.7 Hz, 1H, CH). ¹³C NMR (75 MHz, CDCl₃): δ_{C} 162.6, 149.6 (q, ²J_{CF} = 34.9 Hz), 144.6, 129.4 (d, ³J_{CF} = 5.6 Hz), 128.3 (q, ²J_{CF} = 30.2 Hz), 126.4, 126.2, 125.4, 122.4, 122.2, 97.6, 79.2, 70.8, 67.0, and 19.3.

General procedure for the coupling of azido DHPMs to acetylenic quinolines

The general procedure for the click chemistry used for coupling azido DHPMs to acetylenic quinolines is described below using **10 h** as an example.

9d (0.19 g, 0.60 mmol) and **3** (0.13 g, 0.60 mmol) were dissolved in 3.0 mL DMF. To this mixture was added freshly prepared 1-M aqueous solution of Na ascorbate (240.0 μ L, 0.24 mmol) and CuSO₄ (120.0 μ L, 0.12 mmol) in sequential. The reaction mixture was stirred at ambient temperature overnight. The mixture was poured into distilled water (25.0 mL) and extracted with EtOAc (3 \times 10.0 mL). The organic layers were combined and washed with brine (10.0 mL), distilled water (5 \times 10.0 mL), dried with MgSO₄, and filtered. The filtrate was concentrated in vacuo to give the crude product, which was purified on column chromatography with SiO₂ using 6% MeOH in DCM as the eluent. See the supplementary information for the full characterisations of the final compounds.

Supplementary Information The online version contains supplementary material available at <https://doi.org/10.1007/s11224-023-02142-y>.

Acknowledgements The authors would also like to thank the Centre for High Performance Computing (CHPC, Cape Town, South Africa) for access to CHPC Lengau Cluster and Schrödinger molecular docking software.

Author contribution All authors contributed to the study. Conception and design, material preparation, data collection, and analysis were performed by Rasheed A. Adigun, Frederick P. Malan, Mohammed O. Balogun, and Natasha October. The first draught of the manuscript was written by Rasheed A. Adigun, and all authors commented on previous versions of the manuscript. All authors read and approved the final manuscript.

Funding Open access funding provided by University of Pretoria. This work was supported by the National Research Foundation (South Africa) (Grant number: 105152) and the University of Pretoria, South Africa (doctoral financial support to Rasheed A. Adigun).

Availability of data and materials Some of the datasets generated during and/or analysed during the current study are in the manuscripts while the rest are available from the corresponding authors on reasonable request.

Declarations

Ethics approval Not applicable.

Competing interests The authors declare no competing interests.

Open Access This article is licensed under a Creative Commons Attribution 4.0 International License, which permits use, sharing, adaptation, distribution and reproduction in any medium or format, as long as you give appropriate credit to the original author(s) and the source, provide a link to the Creative Commons licence, and indicate if changes were made. The images or other third party material in this article are included in the article's Creative Commons licence, unless indicated

otherwise in a credit line to the material. If material is not included in the article's Creative Commons licence and your intended use is not permitted by statutory regulation or exceeds the permitted use, you will need to obtain permission directly from the copyright holder. To view a copy of this licence, visit <http://creativecommons.org/licenses/by/4.0/>.

References

1. WHO, World Malaria Report (2019) <https://www.who.int/malaria>, <https://www.who.int/publications-detail/world-malaria-report-2019>
2. Menezes CMS, Ferreira EI (2005) Modulating agents in resistant malaria. *Drug Des Rev Online* 2:409–418. <https://doi.org/10.2174/1567269054546433>
3. Hu Y-QQ, Gao C, Zhang S, Xu L, Xu Z, Feng LS, Wu X, Zhao F (2017) Quinoline hybrids and their antiplasmodial and antimalarial activities. *Eur J Med Chem* 139:22–47. <https://doi.org/10.1016/j.ejmech.2017.07.061>
4. Van DA, Schalkwyk JC, Walden PJ (2001) Smith, Reversal of chloroquine resistance in Plasmodium falciparum using combinations of chemosensitizer. *Antimicrob Agents Chemother* 45:3171–3174. <https://doi.org/10.1128/AAC.45.11.3171>
5. Wright DJ, O'Reilly M, Tisi D (2018) Engineering and purification of a thermostable, high-yield, variant of PfCRT, the Plasmodium falciparum chloroquine resistance transporter. *Protein Expr Purif* 141:7–18. <https://doi.org/10.1016/j.pep.2017.08.005>
6. Martin SK, Oduola AM, Milhous WK (1987) Reversal of chloroquine resistance in Plasmodium falciparum by verapamil. *Science* 235:899–901. <https://doi.org/10.1126/science.3317830>
7. Alibert-Franco S, Pradines B, Mahamoud A, Davin-Regli A, Pages J-M (2008) Efflux mechanism, an attractive target to combat multidrug resistant Plasmodium falciparum and Pseudomonas aeruginosa. *Curr Med Chem* 16:301–317. <https://doi.org/10.2174/092986709787002619>
8. Egan TJ, Kaschula CH (2007) Strategies to reverse drug resistance in malaria. *Curr Opin Infect Dis* 20:598–604. <https://doi.org/10.1097/QCO.0b013e3282f1673a>
9. Warhurst DC (2003) Polymorphism in the Plasmodium falciparum chloroquine-resistance transporter protein links verapamil enhancement of chloroquine sensitivity with the clinical efficacy of amodiaquine. *Malar J* 2:1–12. <https://doi.org/10.1186/1475-2875-2-1>
10. Henry M, Alibert S, Orlandi-Pradines E, Bogreau H, Fusai T, Rogier C, Barbe J, Pradines B (2006) Chloroquine resistance reversal agents as promising antimalarial drugs. *Curr Drug Targets* 7:935–948. <https://doi.org/10.2174/138945006778019372>
11. Krogstad DJ, Gluzman IY, Kyle DE, Oduola AM, Martin SK, Milhous WK, Schlesinger PH (1987) Efflux of chloroquine from Plasmodium falciparum: mechanism of chloroquine resistance. *Science* 238:1283–1285. <https://doi.org/10.1126/science.3317830>
12. Millet J, Torrentino-Madamet M, Alibert S, Rogier C, Santelli-Rouvrier C, Mosnier J, Baret E, Barbe J, Parzy D, Pradines B (2004) Dihydroethanoanthracene derivatives as in vitro malarial chloroquine resistance reversal agents. *Antimicrob Agents Chemother* 48:2753–2756. <https://doi.org/10.1128/aac.48.7.2753-2756.2004>
13. Kyle DE, Oduola AMJJ, Martin SK, Milhous WK (1990) Plasmodium falciparum: modulation by calcium antagonists of resistance to chloroquine, desethylchloroquine, quinine, and quinidine in vitro. *Trans R Soc Trop Med Hyg* 84:474–478. [https://doi.org/10.1016/0035-9203\(90\)90004-X](https://doi.org/10.1016/0035-9203(90)90004-X)
14. Burgess SJ, Selzer A, Kelly JX, Smilkstein MJ, Riscoe MK, Peyton DH (2006) A chloroquine-like molecule designed to

- reverse resistance in *Plasmodium falciparum*. *J Med Chem* 49:5623–5625. <https://doi.org/10.1021/jm060399n>
15. October N, Watermeyer ND, Yardley V, Egan TJ, Ncokazi K, Chibale K (2008) Reversed chloroquinones based on the 3,4-dihydropyrimidin-2(1H)-one scaffold: synthesis and evaluation for antimalarial, β -haematin inhibition, and cytotoxic activity. *ChemMedChem* 3:1649–1653. <https://doi.org/10.1002/cmdc.200800172>
 16. Kaur K, Jain M, Reddy RP, Jain R (2010) Quinolines and structurally related heterocycles as antimalarials. *Eur J Med Chem* 45:3245–3264. <https://doi.org/10.1016/j.ejmech.2010.04.011>
 17. Becker K, Rahlfs S, Nickel C, Schirmer RH (2003) Glutathione–functions and metabolism in the malarial parasite *Plasmodium falciparum*. *Biol Chem* 384:551–566
 18. Kamaria P, Kawathekar N (2014) Ligand-based 3D-QSAR analysis and virtual screening in exploration of new scaffolds as *Plasmodium falciparum* glutathione reductase inhibitors. *Med Chem Res* 23:25–33. <https://doi.org/10.1007/s00044-013-0603-7>
 19. Fagan RL, Palfey BA (2010) 7.03 - Flavin-dependent enzymes, In: Ben HW, Liu LBT, Mander CNP (ed) *Comprehensive Natural Products II Chemical Biology*, Elsevier, Oxford, p 37–113. <https://doi.org/10.1016/B978-008045382-8.00135-0>
 20. Pastrana-Mena R, Dinglasan RR, Franke-Fayard B, Vega-Rodríguez J, Fuentes-Caraballo M, Baerga-Ortiz A, Coppens I, Jacobs-Lorena M, Janse CJ, Serrano AE (2010) Glutathione reductase-null malaria parasites have normal blood stage growth but arrest during development in the mosquito. *J Biol Chem* 285:27045–27056
 21. Adigun RA, Malan FP, Balogun MO, October N (2021) Substitutional effects on the reactivity and thermal stability of dihydropyrimidinones. *J Mol Struct* 1223:129193. <https://doi.org/10.1016/j.molstruc.2020.129193>
 22. Fisher GM, Tanpure RP, Douchez A, Andrews KT, Poulsen S-A (2014) Synthesis and evaluation of antimalarial properties of novel 4-aminoquinoline hybrid compounds. *Chem Biol Drug Des* 84:462–472. <https://doi.org/10.1111/cbdd.12335>
 23. Kaval N, Ermolat'ev D, Appukkuttan P, Dehaen W, Kappe CO, Van der Eycken E (2005) The application of “click chemistry” for the decoration of 2(1h)-pyrazinone scaffold: generation of templates. *J Comb Chem* 7:490–502. <https://doi.org/10.1021/cc0498377>
 24. Eswaran S, Vasudeva A, Chowdhury IH, Pal NK, Thomas KD (2010) New quinoline derivatives: synthesis and investigation of antibacterial and antituberculosis properties. *Eur J Med Chem* 45:3374–3383. <https://doi.org/10.1016/j.ejmech.2010.04.022>
 25. Mao J, Yuan H, Wang AY, Wan B, Pieroni M, Huang Q, Van Breemen RB, Kozikowski PA, Scott GF (2009) From serendipity to rational antituberculosis drug discovery of mefloquine-isoxazole carboxylic acid esters. *J Med Chem* 52:6966–6978. <https://doi.org/10.1021/jm900340a>
 26. Lilienkamp A, Jialin M, Baojie W, Yuehong W, Franzblau SG, Kozikowski AP (2009) Structure-activity relationships for a series of quinoline-based compounds active against replicating and nonreplicating *Mycobacterium tuberculosis*. *J Med Chem* 52:2109–2118. <https://doi.org/10.1021/jm900003c>
 27. Brouet JC, Gu S, Peet NP, Williams JD (2009) Survey of solvents for the Conrad-Limpach synthesis of 4-hydroxyquinolones. *Synth Commun* 39:1563–1569. <https://doi.org/10.1080/00397910802542044>
 28. Li JJ (2014) *Name reactions: a collection of detailed mechanisms and synthetic applications*, 5th ed. Springer, Science and Business Media
 29. Sarojini BK, Narayana B, Mayekar AN, Yathirajan HS, Bolte M (2007) A 1:1 cocrystal of 2,8-bis-(trifluoro-methyl)quinolin-4-ol and 2,8-bis-(tri-fluoromethyl)quinolin-4(1H)-one, *Acta Crystallogr. Sect E Struct Reports Online* 63:7–13. <https://doi.org/10.1107/S1600536807053482>
 30. Keto-enol tautomerism : key points - Master Organic Chemistry (nd) <https://www.masterorganicchemistry.com/2022/06/21/keto-enol-tautomerism-key-points/> (accessed 25 January 2023)
 31. Guantai EM, Ncokazi K, Egan TJ, Gut J, Rosenthal PJ, Smith PJ, Chibale K (2010) Design, synthesis and in vitro antimalarial evaluation of triazole-linked chalcone and dienone hybrid compounds, *Bioorganic. Med Chem* 18:8243–8256. <https://doi.org/10.1016/j.bmc.2010.10.009>
 32. Chu XM, Wang C, Wang WL, Liang LL, Liu W, Gong KK, Sun KL (2019) Triazole derivatives and their antiplasmodial and antimalarial activities. *Eur J Med Chem* 166:206–223. <https://doi.org/10.1016/j.ejmech.2019.01.047>
 33. Chopra R, Chibale K, Singh K (2018) Pyrimidine-chloroquinoline hybrids: synthesis and antiplasmodial activity. *Eur J Med Chem* 148:39–53. <https://doi.org/10.1016/j.ejmech.2018.02.021>
 34. Natarajan JK, Alumasa JN, Yearick K, Ekoue-Kovi KA, Casabianca LB, De Dios AC, Wolf C, Roepe PD (2008) 4-N-, 4-S-, and 4-O-chloroquine analogues: influence of side chain length and quinolyl nitrogen pKa on activity vs chloroquine resistant malaria. *J Med Chem* 51:3466–3479. <https://doi.org/10.1021/jm701478a>
 35. Taleli L, De Kock C, Smith PJ, Pelly SC, Blackie MAL, Van Otterlo WAL (2015) In vitro antiplasmodial activity of triazole-linked chloroquinoline derivatives synthesised from 7-chloro-N-(prop-2-yn-1-yl)quinolin-4-amine. *Bioorg Med Chem* 23:4163–4171. <https://doi.org/10.1016/j.bmc.2015.06.044>
 36. Slater AFG (1993) Chloroquine: mechanism of drug action and resistance in *plasmodium falciparum*. *Pharmacol Ther* 57:203–235. [https://doi.org/10.1016/0163-7258\(93\)90056-J](https://doi.org/10.1016/0163-7258(93)90056-J)
 37. Joshi MC, Wicht KJ, Taylor D, Hunter R, Smith PJ, Egan TJ (2013) In vitro antimalarial activity, β -haematin inhibition and structure-activity relationships in a series of quinoline triazoles. *Eur J Med Chem* 69:338–347. <https://doi.org/10.1016/j.ejmech.2013.08.046>
 38. Adigun RA, Malan FP, Balogun MO, October N (2022) Rational optimization of dihydropyrimidinone-quinoline hybrids as *Plasmodium falciparum* glutathione reductase inhibitors. *ChemMedChem* 17:1–15. <https://doi.org/10.1002/cmdc.202200034>
 39. Mensah JO, Ampomah GB, Gasu EN, Adomako AK, Menkah ES, Borquaye LS (2022) Allosteric modulation of the main protease (MPro) of SARS-CoV-2 by casticin—insights from molecular dynamics simulations. *Chem Africa* 5:1305–1320. <https://doi.org/10.1007/s42250-022-00411-7>
 40. Kalibaeva G, Ferrario M, Ciccotti G (2003) Constant pressure-constant temperature molecular dynamics: a correct constrained NPT ensemble using the molecular virial. *Mol Phys* 101:765–778
 41. Martyna GJ (1994) Remarks on “‘Constant-temperature molecular dynamics with momentum conservation’.” *Phys Rev E* 50:3234
 42. APEX3 (including SAINT and SADABS) (2016) Bruker AXS Inc. Madison, WI
 43. Rigaku Oxford Diffraction (2018) CrysAlisPro software system
 44. Sheldrick GM (2015) SHELXT - integrated space-group and crystal-structure determination. *Acta Crystallogr Sect A Found Crystallogr* 71:3–8. <https://doi.org/10.1107/S2053273314026370>
 45. Sheldrick GM (2015) Crystal structure refinement with SHELXL, *Acta Crystallogr. Sect C Struct Chem C* 71:3–8

Publisher's Note Springer Nature remains neutral with regard to jurisdictional claims in published maps and institutional affiliations.